Redox Biology 46 (2021) 102076

Contents lists available at ScienceDirect

Redox Biology

journal homepage: www.elsevier.com/locate/redox

The cross-talk between tumor cells and activated fibroblasts mediated by lactate/BDNF/TrkB signaling promotes acquired resistance to anlotinib in human gastric cancer

Zhijian Jin [a,1], Yifan Lu [a,1], Xiongyan Wu [a,1], Tao Pan [a], Zhenjia Yu [a], Junyi Hou [a], Airong Wu [b], Jianfang Li [a], Zhongyin Yang [a], Chen Li [a], Min Yan [a], Chao Yan [a], Zhenggang Zhu [a], Bingya Liu [a], Weihua Qiu [a,**], Liping Su [a,*]

[a] Department of General Surgery, Ruijin Hospital, Shanghai Jiao Tong University School of Medicine, Shanghai, 200025, China
[b] Department of Gastroenterology, The First Affiliated Hospital of Soochow University, 188 Shizi Street, Suzhou, 215006, Jiangsu, China

ARTICLE INFO

Keywords:
Fibroblast
Anlotinib
BDNF
TrkB
ROS
Nrf2

ABSTRACT

Acquired resistance to tyrosine kinase inhibitors (TKIs) is the major obstacle to improve clinical efficacy in cancer patients. The epithelial-stromal interaction in tumor microenvironment influences cancer drug response to TKIs. Anlotinib is a novel oral multi-targeted TKI, and has recently been proven to be effective and safe for several tumors. However, if and how the epithelial-stromal interaction in tumor microenvironment affects anlotinib response in gastric cancer (GC) is not known. In this study, we found that anlotinib inhibited GC cells growth by inducing GC cells apoptosis and G2/M phase arrest in a dose- and time-dependent manner. Reactive oxygen species (ROS) mediated anlotinib-induced apoptosis in GC cells, while cancer-associated fibroblasts (CAFs) significantly suppressed anlotinib-induced apoptosis and ROS in GC cells. Increased BDNF that was derived from CAFs activated TrkB-Nrf2 signaling in GC cells, and reduced GC cells response to anlotinib. We identified secreted lactate from GC cells as the key molecule instructing CAFs to produce BDNF in a NF-κB-dependent manner. Additionally, functional targeting BDNF-TrkB pathway with neutralizing antibodies against BDNF and TrkB increased the sensitivity of GC cells towards anlotinib in human patient-derived organoid (PDO) model. Taken together, these results characterize a critical role of the epithelial-stroma interaction mediated by the lactate/BDNF/TrkB signaling in GC anlotinib resistance, and provide a novel option to overcome drug resistance.

1. Introduction

Gastric cancer (GC) is one of the most common types of cancers in both men and women, ranking fifth for incidence and fourth for mortality globally [1]. Targeted therapy is one of the major modalities of medical treatment for advanced GC, with high selectivity and minimal effects. Tyrosine kinase inhibitors (TKIs) are one of the most common targeted drug, and have been wildly used in advanced GC. Despite the development in treatment, patients with GC respond poorly to TKI, which is mainly due to drug resistance. Therefore, understanding the mechanism that induces resistance is a key challenge in improving the outcome of GC.

Anlotinib is a new oral multi-targeted TKI that targets VEGFR, PDGFR, FGFR, MET, Ret and c-kit [2–5], and has been approved for treating non-small cell lung cancer (NSCLC) [6]. To date, anlotinib has shown the promising antitumor effects on various cancers, including metastatic soft-tissue sarcoma, intrahepatic cholangiocarcinoma, synovial sarcoma, hepatocellular carcinoma, etc. by inhibiting angiogenesis and cell proliferation [4,7–10]. Clinical trials of anlotinib in treating stomach cancer are in progress [11], however, its function and clinical efficacy on GC is still incompletely understood.

Drug resistance remains the major obstacle to achieve optimal outcomes in cancer patients. The clinical efficacy of TKIs is usually limited by the rapid and inevitable development of acquired drug resistance that is associated with tumor cells as well as with the tumor microenvironment (TME). The interactions between cancer cells and TME have been

* Corresponding author.
** Corresponding author.
E-mail addresses: qwh11072@rjh.com.cn (W. Qiu), suliping@shsmu.edu.cn (L. Su).
[1] Zhijian Jin, Yifan Lu and Xiongyan Wu contributed equally to this article.

https://doi.org/10.1016/j.redox.2021.102076
Received 1 June 2021; Received in revised form 8 July 2021; Accepted 19 July 2021
Available online 20 July 2021

demonstrated to be involved in the pathogenesis of multiple cancer types. Mounting evidences have demonstrated that intra-tumoral stroma proportion is associated with poor prognosis of gastric cancer [12,13]. Cancer-associated fibroblasts (CAFs) are the main cell type constituting tumor stroma in TME. CAFs actively communicate with cancer cells, and contribute to tumor progression by providing growth niche, promoting immune evasion or inducing chemoresistance [14–16]. We have previously shown that CAFs promote GC cells proliferation and metastatic ability through secreting IL6, HGF and IL33 [17–19]. However, whether CAFs regulate GC cells response to anlotinib and its underlying molecular mechanisms remain unknown.

In the present study, we examined the anti-tumor effects of anlotinib on GC cells and determined the epithelial-stromal interaction in regulating the response to anlotinib in GC. We find that anlotinib promotes GC cells apoptosis through elevated ROS, and co-culture with CAFs results in reduced sensitivity to anlotinib in GC cells. Moreover, we demonstrate that CAFs-derived BDNF mediates sensitivity to anlotinib in GC via activation of the TrkB/Nrf2 pathway, and in turn, GC cells-derived lactate upregulates BDNF expression in CAFs through activation of NF-κB pathway. Furthermore, CAFs significantly reduce the efficacy of anlotinib to GC in xenograft tumor model and patient-derived organoid model, and interfering BDNF/TrkB pathway restores tumor sensitivity to anlotinib. Thus, we identify lactate/BDNF/TrkB signaling as a mediator of the tumor-stromal cell interaction in anlotinib resistance, and increased production of tumor lactate and stromal BDNF may be potentially targeted adaptive alterations.

2. Materials and methods

2.1. Cell culture and patient samples

GC cell line AGS used in our study was purchased from the American Type Culture Collection (ATCC), and MGC-803, HGC-27 and GES-1 cell lines were purchased from Shanghai Institutes for Biological Sciences, Chinese Academy of Sciences. All GC cell lines were authenticated by short-tandem repeat analysis and had negative results for mycoplasma. CAFs were isolated and cultured from GC tissues as described in our previous study [18]. AGS and HGC-27 were cultured at 37 °C in a humidified atmosphere of 5% CO_2 with RPMI-1640 medium containing 10% fetal bovine serum with 100 U/ml penicillin and 100 U/ml streptomycin. MGC-803 and CAFs were cultured at 37 °C in a humidified atmosphere of 5% CO2 with Dulbecco's Modified Eagle Medium (DMEM) containing 10% fetal bovine serum with 100-U/ml penicillin and 100-U/ml streptomycin. The reagents were listed in Table S1.

A total of 178 GC patients in this study underwent radical gastrectomy at Shanghai Ruijin Hospital. All samples were obtained with the patients' informed consent, and the samples were histologically confirmed.

2.2. Cell viability and colony formation assay

The Cell Counting Kit-8 (CCK-8, Dojindo, Kumamoto, Japan) was used for the cell proliferation assay. In brief, cells were plated in 96-well plates at 5×10^3 cells per well 24 h before treatment. The cells were treated with indicated drugs or intervention for 24, 48, or 72 h. Cell viability was quantified by measuring the absorbance at 450 nM through microplate reader (Epoch; BioTek, Winooski, VT). The median inhibitory concentration (IC50) was calculated using Prism 8.3.1 software (GraphPad Software). For the colony formation assay, 1000 cells were plated per well in 6-well plates and cultured at 37 °C with 5% CO2 for 14 days. Colony formation was detected by staining with 0.1% crystal violet in methanol for 30 min.

2.3. EdU detection

An EdU dye assay was performed using the EdU Cell Proliferation Kit with Alexa Fluor 594 (Beyotime Biotechnology, Shanghai, China) according to the manufacturer's instructions. The labeled cells were detected by a fluorescence microscope (Life Technologies, ThermoFisher Scientific, USA), and analyzed by Image-pro-plus 6.0 software (Media Cybernetics, Inc., MD, USA). The results were calculated by the following equation: Percentage of cells (%) = The count of EdU cells/ The count of total cells × 100%.

2.4. Cell apoptosis and cell cycle analysis

Flow cytometric assays of apoptosis and cell cycle were performed as previously described [20]. Briefly, both attached and floating cells were harvested, washed twice with ice-cold PBS and suspended in 100 μl binding buffer. Cells were incubated with 3 μl FITC-Annexin V and 5 μl PI at room temperature for 15 min in the dark. Next, an additional 300 μl 1 × Binding Buffer was added to each sample, and then apoptosis was analyzed by flow cytometry (FACSCalibur; Becton Dickinson, Sparks, MD). For cell cycle analysis, single-cell suspension was fixed with 70% cold ethanol at 4 °C overnight. Afterwards, samples were washed twice with cold PBS, incubated with PI (50 μg/ml) at 37 °C for 30 min in the dark, and then analyzed by flow cytometry (FACSCalibur).

2.5. Reactive oxygen species (ROS) detection

Intracellular ROS levels were evaluated using a 2, 7-dichlorofluorescein diacetate-based ROS Assay Kit (Beyotime Biotechnology, Shanghai, China), in accordance with the manufacturer's instructions. In brief, at the end of the experiment, cells were incubated with serum-free medium containing 0.1% DCFH-DA and protected from light at 37 °C for 20 min. Fluorescence was detected by a FACS Calibur flow cytometer (Becton-Dickinson, San Jose, CA, USA).

2.6. Quantitative real-time PCR (qRT-PCR)

Total RNA was extracted using Trizol reagent (Invitrogen, Carlsbad, CA, USA) following the manufacturer's manual. RNA (1 μg) was reverse transcribed into cDNA using Reverse Transcription system (Promega, Madison, WI, USA). QRT-PCR was performed to quantify the mRNA levels of BDNF, NTF4, RNASE7, HO-1 and Nrf2 with the SYBR Green PCR core Reagent kit (Applied Biosystems, Foster City, CA, USA). Data were analyzed by using the comparative Ct method. Specificity of resulting PCR products was confirmed by melting curves. The primers used in this assay were listed in Table S2.

2.7. Enzyme-linked immunosorbent assay (ELISA)

The protein levels of BDNF in supernatants were measured by an ELISA kit (R&D Systems, Minneapolis, MN, USA) according to the manufacturer's instructions.

2.8. Immunofluorescence

Cells were fixed for 30 min with 4% paraformaldehyde and rinsed with phosphate buffered saline (PBS). Cells were then blocked with normal nonimmune goat serum for 30 min prior to being incubated with primary antibodies (listed in Table S3) at 37 °C for 2 h. After rinses with PBS, cells were stained with appropriate Alexa dye-conjugated secondary immune reagents, and DAPI. Negative control staining was performed by omission of the primary antibody.

2.9. Isolation of nuclear and cytoplasmic extract

The nuclear extraction was prepared using an NE-PER Nuclear Cytoplasmic Extraction Reagent kit (Pierce, Rockford, IL, USA) according to the manufacturer's instruction. Briefly, the treated cells were washed twice with cold PBS and centrifuged at 500 g for 3 min. The cell

pellet was suspended in 200 ml of cytoplasmic extraction reagent I by vortexing. The suspension was incubated on ice for 10 min followed by the addition of 11 μl of a second cytoplasmic extraction reagent II, vortexed for 5 s, incubated on ice for 1 min and centrifuged for 5 min at 16 000 g. The supernatant fraction (cytoplasmic extract) was transferred to a pre-chilled tube. The insoluble pellet fraction, which contains crude nuclei, was resuspended in 100 μl of nuclear extraction reagent by vortexing during 15 s and incubated on ice for 10 min, then centrifuged for 10 min at 16 000 g. The resulting supernatant, constituting the nuclear extract, was used for the subsequent experiments.

2.10. Immunohistochemistry (IHC)

IHC was performed as described previously [20]. The percentage of positive cells was classified into four grades (percentage scores): 0% (0), 1–30% (1), 31–60% (2), 61–100% (3). The staining intensity was classified into four grades (intensity scores): no staining (0), light brown staining (1), brown staining (2), dark brown staining (3). We multiplied the percentage scores and intensity scores to get total scores: weak positive (0–3), strong positive (≥4).

2.11. Immunoprecipitation and immunoblot analyses

Immunoprecipitation analyses were performed using the Direct Magnetic IP/Co-IP Kit (ThermoFisher, 88828) according to the manual. Briefly, indicated antibodies were bound to the beads for 60 min. Cell lysates were incubated with antibody-bound beads overnight at 4 °C. Washed the beads twice with Wash Buffer and once with ultrapure water. Eluted bound antigen.

For Western blot analyses, the cells were digested in RIPA buffer with presence of Protease Inhibitor Cocktail (ThermoFisher, 87785). Protein concentration was quantified using the BCA Protein Assay Kit (ThermoFisher, 23227). After electrophoresis in SDS-PAGE, the proteins were transferred to PVDF membranes (Bio-Rad, 1620177). After blocking with 5% nonfat milk, blots were immunoblotted with the indicated primary antibodies (listed in Table S3).

2.12. Enzymatic chromatin immunoprecipitation assay

Enzymatic chromatin immunoprecipitation (ChIP) assays were performed using the Enzymatic ChIP Kit (Cell Signaling Technology, #9005) according to the manual. Briefly, cells were cross-linked in 1% formaldehyde solution for 10 min at room temperature, followed by the addition of 125 mM of glycine for 5 min. Antibodies including anti-p65 and normal IgG were used for each immunoprecipitation. Immunoprecipitated and input DNAs were subjected to qRT-PCR analyses. The primers used for amplification are listed in Supplementary Table S2.

2.13. Fluorescence in situ hybridization (FISH)

For the fluorescent probes, Cy3 was used as the marker for α-SMA, and FAM was used as the marker for BDNF. 4′,6-Diamidino-2-phenylindole (DAPI) was used to stain nuclei. FISH was performed according to the instructions of the FISH kit (GenePharma, China). The stained cells were then visualized using a confocal microscope (Leica, Germany).

2.14. Dual luciferase reporter assays

Dual luciferase reporter assays were performed as described previously [21]. Briefly, BDNF promoter fragments were amplified and cloned into the pGL3 basic vector. Luciferase activity was examined using a Dual Luciferase Assay (Promega, Madison, WI, USA) following the manufacturer's instructions.

2.15. Xenograft tumor model

Four-week-old male BALB/c nude mice were purchased from the Institute of Zoology Chinese Academy of Sciences and housed at a specific pathogen-free environment in the Animal Laboratory Unit, Ruijin Hospital, China. All experiments were performed in accordance with the official recommendations of the Chinese Zoological Society, and animals received humane care according to the criteria outlined in the "Guide for the Care and Use of Laboratory Animals". A suspension containing 1×10^6 MGC-803 cells with or without 2.5×10^5 CAFs was subcutaneously injected into right flanks of the nude mice. After 10 days, all mice were randomly divided and received indicated treatment. The tumor dimensions were measured using a Vernier caliper once per week.

2.16. Establishment and culture of PDOs from GC cancers

Briefly, tumor tissue was minced, and digested in a rotating shaker with enzyme mix (Miltenyi Biotec, 130-095-929) at 37 °C. Following digestion, mechanical force (pipetting) was applied in order to facilitate cell release in solution. Dissociated cells were resuspended in 50 μl 50% Matrigel (Corning) and seeded in 24-well flat bottom cell culture plate (Corning). The matrigel was then solidified by a 30-min incubation in a 37 °C and 5% CO_2 cell culture incubator, and overlaid with 750 μl of Organoid Growth Medium (StemCell Technologies, 06010) with 10 μM Y-27632 (Sigma-Aldrich), 100 U/ml penicillin and 100 U/ml streptomycin for establishment of organoids, complete media was subsequently refreshed every three days.

Passaging of PDOs was performed using TrypLe. Briefly, PDOs were mechanically harvested (pipetting) out of matrigel using PBS-EDTA 1 mM containing 1x TrypLe, and incubated for 30 min at 37 °C. PDOs were then dissociated to single cells by applying mechanical force (pipetting), washed with HBSS (Thermo Fisher Scientific), pelleted (200 g, 5 min, 4 °C), resuspended in matrigel, and re-seeded at an appropriate ratio.

PDOs were biobanked in FBS (Thermo Fisher Scientific), containing 10% DMSO (Sigma-Aldrich).

2.17. Proliferation and apoptosis assays of organoid

For transwell co-cultures, 2×10^4 CAFs were seeded in Matrigel on top of the transwell membrane (Millipore) with organoids growing in the lower compartment in 24-well plates. After indicated treatment, proliferation was measured by CellTiter-Glo 3D Cell Viability Assay (G9681; Promega), and apoptosis was detected by RealTime-Glo Annexin V Apoptosis and Necrosis Assay (JA1011; Promega).

2.18. Statistical analyses

All experiments were repeated at least three times, and the results were summarized as means ± SD. Student *t*-test and one-way analysis of variance (ANOVA) were used to analyze the data and Chi-square tests were used to analyze categorical variables. P values < 0.05 were regarded as indicating statistically significant differences ($^*p < 0.05$, $^{**}p < 0.01$).

3. Results

3.1. Anlotinib inhibits the growth of gastric cancer cells by inducing apoptosis and G2/M phase arrest in vitro

To detect the effect of anlotinib on GC cell growth, three GC cell lines (MGC-803, HGC-27 and AGS) were treated with anlotinib at different concentrations for indicated times. We found that anlotinib significantly inhibited GC cells viability in a dose- and time-dependent manner evaluated by CCK-8 assay (Fig. 1A). The IC50 values of the three cell lines with anlotinib for 24h, 48h or 72h were shown in Fig. 1A. Moreover, colony formation was performed to detect the anti-proliferation

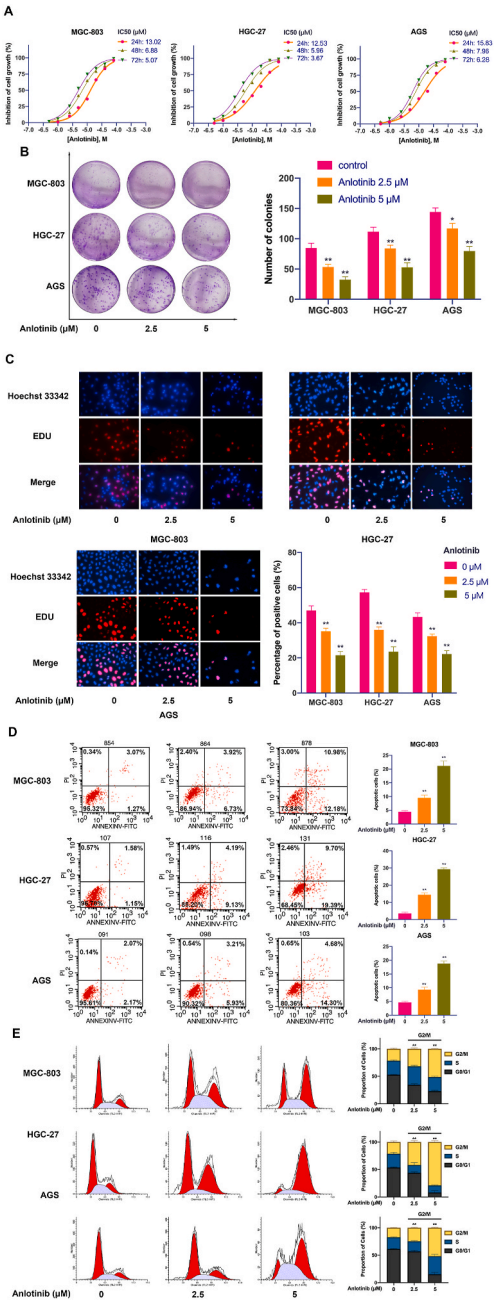

Fig. 1. Anlotinib inhibits the proliferation, induces apoptosis and G2/M phase arrest of GC cells. A. Dose- and time-dependent curves showing the percentage of inhibition of GC cells. MGC-803, HGC-27 and AGS cells were treated with various concentrations of anlotinib (0–80 μM) for 24, 48 or 72 h. A CCK-8 assay was used to determine the viability of GC cells. **B.** Representative images of colony formation assay. **C.** Representative images of EdU staining of GC cells after anlotinib treatment for 24 h (200 ×). **D.** The ratio of apoptotic cells was measured in MGC-803, HGC-27 and AGS cells after anlotinib treatment for 24 h. Apoptosis was detected by Annexin V-FITC and propidium iodide (PI) staining. **E.** Anlotinib-induced G2/M phase arrest in GC cells. The cells were treated with anlotinib for 24 h and analyzed by flow cytometry after staining with PI. The data are presented as the mean ± SD from three independent experiments (*$p < 0.05$; **$p < 0.01$).

effects of anlotinib on GC cells. The results showed fewer clone number in MGC-803, HGC-27 and AGS cells after anlotinib treatment (Fig. 1B). Also, DNA replication in the GCs was analyzed by the incorporation of 5-ethynyl-2′-deoxyuridine (EDU) to further confirm the effect of anlotinib in inhibition of GC cell proliferation. As shown in Fig. 1C, after treated by anlotinib for 24h, the incorporation of EDU in MGC-803, HGC-27 or AGS cells was significantly decreased when compared with the control group. These results indicate that anlotinib elicits anti-proliferation effects on GC cells *in vitro*.

To investigate the mechanism of the anti-proliferation effects of anlotinib on GC, the apoptosis was evaluated by flow cytometry. The results showed that anlotinib treatment induced GC cell apoptosis, and the apoptotic rates were increased in a dose-dependent manner (Fig. 1D). Furthermore, the distribution of the cell cycle was evaluated. As shown in Fig. 1E, after treated with anlotinib for 24h, the percentage of GC cells in G2/M phase was significantly increased in a dose-dependent manner. These results indicate that anlotinib induces GC cell apoptosis and G2/M phase arrest, which contributes to its growth inhibitory effects in human GC.

3.2. *Reactive oxygen species (ROS) mediates anlotinib-induced apoptosis in GC cells*

ROS-mediated apoptosis is considered as an important molecular mechanism for drug therapy. Therefore, we detected whether ROS are involved in anlotinib-induced apoptosis in GC cells. As shown in Fig. 2A and B and Fig. S1A, anlotinib significantly induced the intracellular production of ROS in GC cells assayed by flow cytometry, and the content of ROS in GC cells increased rapidly as the concentration of anlotinib increased, indicating that anlotinib has the strong potential to induce ROS production in a dose-dependent manner in GC cells. Mitochondria is the main source of cellular ROS. We found that anlotinib treatment significantly impaired mitochondrial respiratory chain complex IV and V function, which may contribute to the accumulation of ROS in GC cells induced by anlotinib (Fig. S1B). In addition, anlotinib also decreased the GSH/GSSG ratio, and the activity of glutathione peroxidase, which could be significantly reversed by N-acetyl-cysteine (NAC), an ROS scavenger (Fig. S1C and S1D).

Mitochondrial membrane potential (MMP) is a key maker of mitochondrial function. The loss of MMP has been considered an early hallmark of mitochondrial dysfunction in apoptotic cells. ROS generation disrupts the MMP, we further studied the effects of anlotinib on MMP in GC cells. MGC-803, HGC-27 and AGS cells were treated with anlotinib and cultured in medium supplemented with or without NAC, and the changes of MMP were monitored by flow cytometry using JC-1 dye. As shown in Fig. 2C, anlotinib significantly reduced MMP of GC cells, which could be diminished by NAC.

Anlotinib-induced ROS production impaired mitochondrial function, and then may cause apoptosis. Therefore, we further determined the role of ROS in anlotinib-induced apoptosis. GC cells were treated with anlotinib and cultured in medium supplemented with or without NAC, and the apoptosis of GC cells was assessed. As shown in Fig. 2D and E, the percentage of apoptotic cells was markedly decreased by NAC combined with anlotinib compared to that of treatment with anlotinib alone. To better understand the cell death pathway induced by ROS accumulation in GC cells, GC cells were treated with anlotinib in the presence of Z-VAD-FMK (inhibitor of caspase) or Ferrostatin-1 (the inhibitor of ferroptosis), and the results revealed that anlotinib-induced inhibition of cell viability could be partially restored by Z-VAD-FMK or Ferrostatin-1. Notably, the restoration of cell viability by Z-VAD-FMK was stronger than that by Ferrostatin-1, indicating that anlotinib-induced cell death was through both apoptosis and ferroptosis, and apoptosis is the main cell death pathway in GC cells treated with anlotinib (Fig. S1E). Thus, these results demonstrate that anlotinib-induced apoptosis is mediated by ROS production in GC cells.

3.3. *CAFs protect GC cells from anlotinib-induced apoptosis and induce resistance to anlotinib*

The clinical efficacy of targeted therapies is usually limited by acquired resistance that is associated with tumor cells and/or TME, we

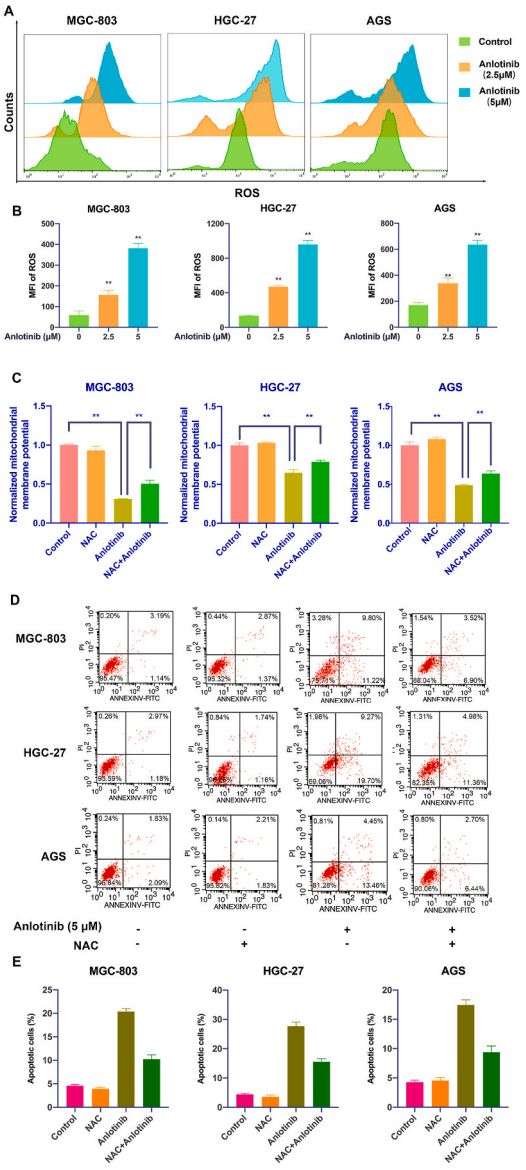

Fig. 2. ROS mediates anlotinib-induced apoptosis in GC cells. A, B. After anlotinib treatment, the ROS levels in GC cells were detected by flow cytometry. **C.** Mitochondrial membrane potential (MMP) was determined and was expressed as JC-1 monomer (green fluorescence)/JC-1 aggregates (red fluorescence) ratio. **D, E.** After treatment with anlotinib and/or NAC, GC cells were stained with PI/Annexin-V-FITC and cell apoptosis was detected by flow cytometry. The data are presented as the mean ± SD from three independent experiments (*$p < 0.05$; **$p < 0.01$). (For interpretation of the references to colour in this figure legend, the reader is referred to the Web version of this article.)

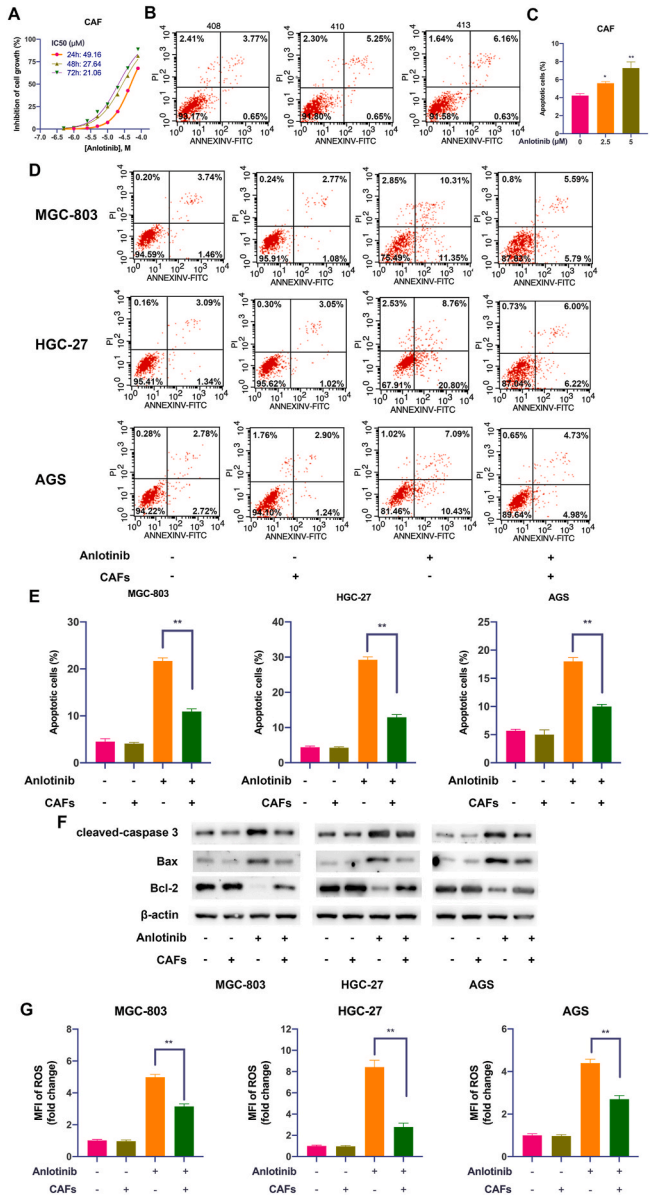

Fig. 3. CAFs protect GC cells from anlotinib-induced apoptosis and induce resistance to anlotinib . A. CCK-8 assay was used to determine the viability of CAFs after anlotinib treatment. **B, C.** Apoptosis of CAFs after anlotinib treatment was detected by PI/Annexin V-FITC staining and flow cytometry. **D, E.** After treatment with anlotinib and/or co-culture with CAFs, and GC cell apoptosis was detected by Annexin V-FITC and propidium iodide (PI) staining. **F.** The expression of cleaved caspase 3, Bax and Bcl-2 in GC cells were detected by Western Blot. **G.** After anlotinib treatment, the ROS levels in GC cells were detected by flow cytometry. The data are presented as the mean ± SD from three independent experiments (*$p < 0.05$; **$p < 0.01$).

therefore determined the regulation of GC cell response to anlotinib in GC microenvironment. CAFs, the major constituent of the tumor stroma, have been demonstrated to contribute to resistance [16]. To determine whether CAFs fuel resistance to anlotinib in GC, we first detected the effects of anlotinib on CAFs. As shown in Fig. 3A–C, although anlotinib inhibited CAFs viability and induced apoptosis in a dose- and time-dependent manner, but the effects of anlotinib on CAFs are significantly lower than that on GC cells (Fig. 1A and D). Furthermore, GC cells were treated with anlotinib and co-cultured with or without CAFs in an *in vitro* transwell co-culture system. The results showed that anlotinib induced apoptosis of GC cells, however, after co-culture with CAFs, the apoptosis of GC cells was significantly decreased ($P < 0.05$), indicating that CAFs strongly impaired the sensitivity to anlotinib in GC cells (Fig. 3D and E). Consistently, the expression of cleaved caspase 3 and Bax were downregulated, and the expression of Bcl-2 was upregulated in anlotinib-treated GC cells after co-cultured with CAFs (Fig. 3F). Meanwhile, the intracellular production of ROS was also restored in anlotinib-treated GC cells after co-cultured with CAFs (Fig. 3G). These results indicate that CAFs reduce the response to anlotinib in GC cells, which might be mediated by soluble factor(s) secreted by CAFs.

3.4. TrkB activation in GC cells is critical for CAFs-mediated anlotinib resistance in GC cells

To determine the molecular mechanism that enables GC cell

resistance to anlotinib induced by CAFs, we detected activation of receptor tyrosine kinase (RTK) by a human RTK phosphorylation array. The result showed that the level of p-TrkB (tropomyosin receptor kinase B, TrkB) and p-ROS1 were significantly elevated in anlotinib-treated GC cells co-cultured with CAFs than without CAFs (Fig. 4A and B). Western Blot analysis revealed that co-culture with CAFs significantly increased the expression of p-TrkB in anlotinib-treated GC cells, while had minor effect on the level of p-ROS1 (Fig. 4C), which suggests TrkB pathway is activated in anlotinib-resistant GC cells induced by CAFs.

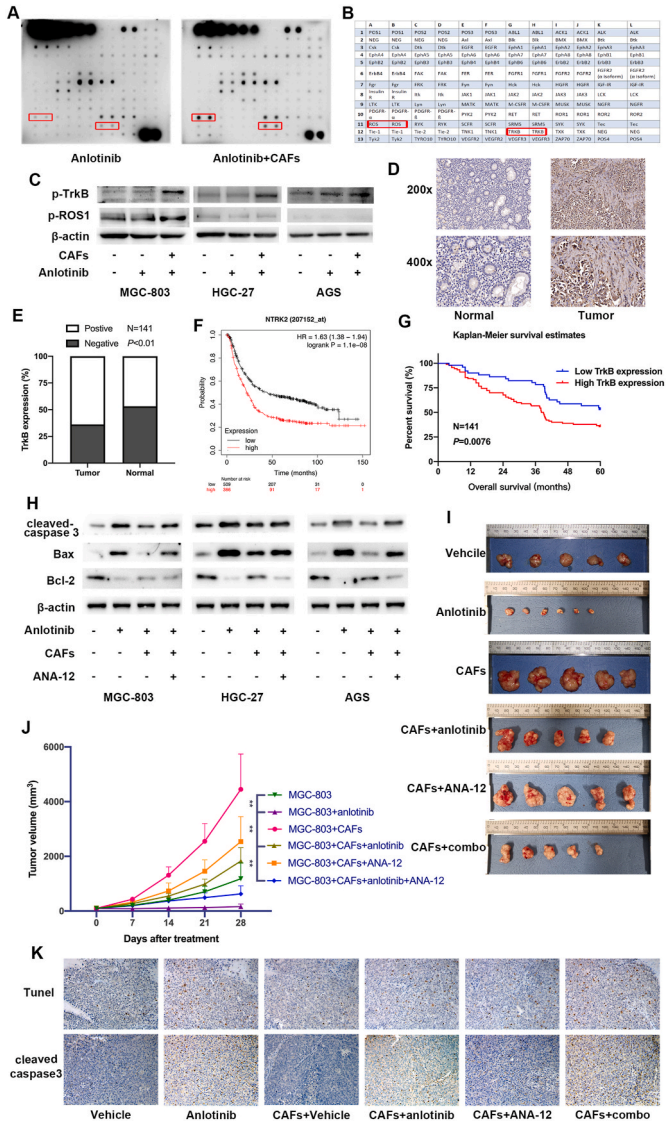

Fig. 4. TrkB activation in GC cells is critical for CAFs-mediated anlotinib resistance in GC cells. A-B. RTK phosphorylation array was performed to detect activation of RTK in GC cells after treatment with anlotinib and/or co-culture with CAFs. **C.** The expression of p-TrkB and p-ROS1 in GC cells treated with anlotinib and/or co-cultured with CAFs were detected by Western Blot. **D.** Representative IHC staining with TrkB antibody in GC tumor tissues and adjacent non-tumor tissues. Magnification: × 200 and × 400. **E.** The positive expression rate of TrkB in tumor tissues and non-tumor tissues. **F.** The overall survival analyses were plotted using Kaplan-Meier Plotter for GC patients with low or high levels of TrkB. **G.** Kaplan-Meier analysis of the overall survival of 141 patients with GC in Ruijin cohort. **H.** After treatment with anlotinib and/or co-culture with CAFs, the expression levels of cleaved caspase3, Bax and Bcl-2 in GC cells were detected by Western Blot. **I-J.** Nude mice were subcutaneously injected with MGC-803 cells alone or mixture of MGC-803 cells and CAFs, and were then treated with anlotinib and/or ANA-12. Tumor volumes were monitored weekly. **K.** Representative images of Tunnel labeling and IHC staining of cleaved caspase 3 on serial sections of tumors from various groups.

TrkB pathway plays an important role in tumorigenesis and cancer metastasis, and accumulating evidence demonstrated that TrkB overexpression is associated with poor survival in patients with various cancer types including GC [22]. To illustrate the expression of TrkB in GC, we analyzed the protein levels of TrkB in 141 pairs of GC tissues and corresponding non-cancerous tissues by immunohistochemistry (IHC). As shown in Fig. 4D, TrkB was strongly expressed in GC tissues compared to non-cancerous tissues, and the positive rate of TrkB protein expression were 63.83% (90/141) in GC tissues and 46.81% (66/141) in non-cancerous tissues (Fig. 4E). Moreover, TrkB mRNA (gene name: NTRK2) level was inversely proportional to survival of 875 GC patients included in GEO, EGA and TCGA databases (Fig. 4F), and Kaplan-Meier survival analysis also revealed that GC patients with high TrkB protein level had a shorter overall survival than with low TrkB protein level (Fig. 4G). Furthermore, inhibition of TrkB activity by adding TrkB inhibitor ANA-12 into the co-culture system led to significantly decreased expression of cleaved caspase 3 and Bax, and increased Bcl-2 in anlotinib-treated GC cells (Fig. 4H), indicating that TrkB activation in GC cells induced by CAFs mediates the protection from anlotinib-induced apoptosis in GC cells.

To confirm the role of TrkB in CAFs-mediated anlotinib resistance *in vivo*, we then subcutaneously injected MGC-803 cells with CAFs into nude mice that were treated with TrkB inhibitor ANA-12 and/or anlotinib. The results showed that anlotinib suppressed tumor growth (MGC-803 + anlotinib vs. MGC-803 group), while CAFs significantly reduced MGC-803 sensitivity to anlotinib *in vivo* (MGC-803 + CAFs + anlotinib vs. MGC-803 + anlotinib group). Although ANA-12 did not significantly impair tumor growth, it markedly prevented the onset of CAFs-induced resistance of anlotinib (MGC-803 + CAFs + anlotinib + ANA12 vs. MGC-803 + CAFs + anlotinib group) (Fig. 4I and J). Furthermore, consistent with the protection from anlotinib-induced apoptosis by CAFs in GC cells, IHC analysis and TUNEL assay verified that there were also decreased expression of cleaved caspase3 and apoptotic cells in subcutaneous tumors derived from MGC-803+CAFs + anlotinib than in tumors derived from MGC-803+anlotinib, which could be impaired by TrkB inhibition by ANA-12 (MGC-803+CAFs + anlotinib + ANA12) (Fig. 4K). Thus, these results suggest that TrkB activation is critical for CAFs-mediated anlotinib resistance in GC cells.

3.5. *Increased BDNF production by CAFs is responsible for protection of GC cells from anlotinib*

Our initial results indicated soluble factor(s) secreted by CAFs might regulate GC cell response to anlotinib. Both BDNF and NTF4 are ligands of TrkB, and RNASE7 is the ligand of ROS1, so we firstly detected the mRNA level of BDNF, NTF4 and RNASE7 in CAFs, and found that CAFs expressed high level of BDNF, but almost not expressed NTF4 and RNASE7 (Fig. 5A). BDNF is a neurotrophic factor that has been shown to stimulate tumor growth and metastasis via specifically binding to TrkB, and overexpression of BDNF in several tumors is associated with resistance to treatment. We therefore considered BDNF may be involve in GC cell resistance to anlotinib. Indeed, GC tumor tissues have higher expression of transcript for BDNF when compared with adjacent normal samples (http://gepia.cancer-pku.cn) (Fig. 5B), and quantitative real-time PCR in 37 pairs of GC tissues also revealed that GC tumor tissues expressed BDNF mRNA at significantly higher levels than corresponding non-cancerous tissues (Fig. 5C). In addition, Kaplan-Meier Plotter analysis (https://kmplot.com/analysis) showed that BDNF expression was inversely proportional to survival of GC patients (Fig. 5D).

To further identify cellular sources that are responsible for the higher expression of BDNF in GC tissues, we detected the co-expression of α-SMA (the marker of CAFs) and BDNF, Cytokeratin (the marker of epithelial cells) or FAP (the marker of CAFs) and TrkB in GC tissues by Fluorescence in situ hybridization (FISH) or immunofluorescence (IF).

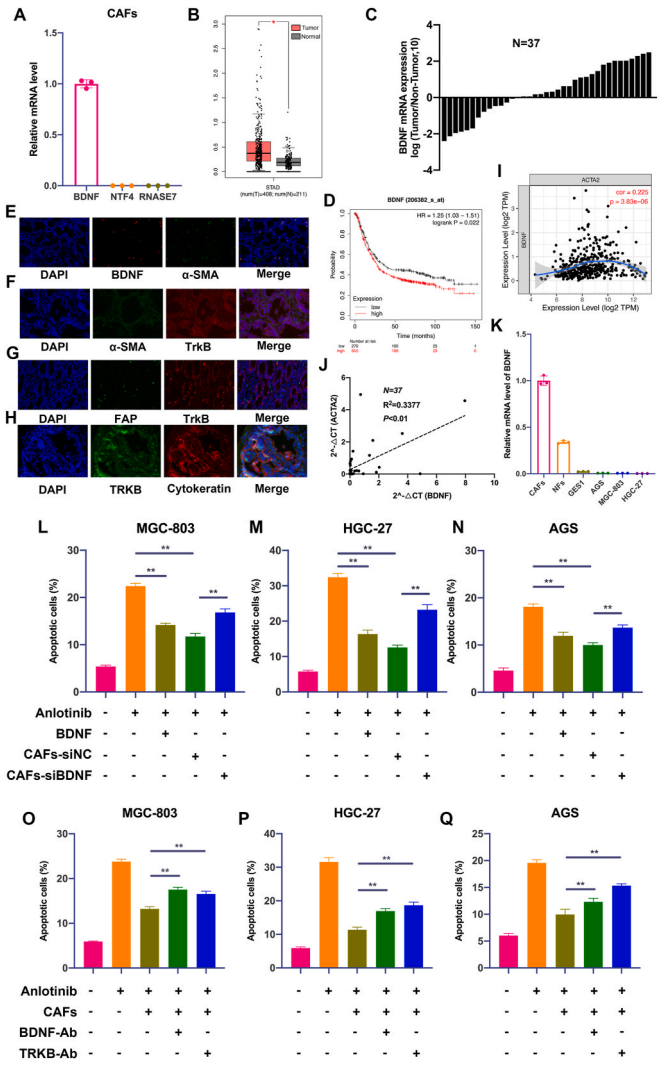

Fig. 5. CAFs-derived BDNF protects GC cells from anlotinib-induced apoptosis. A. The mRNA levels of BDNF, NTF4 and RNASE7 were detected by qRT-PCR in CAFs. **B.** The mRNA level of BDNF in GC samples and normal samples from TCGA data. **C.** QRT-PCR analysis of BDNF mRNA expression in GC tumor tissues and adjacent non-tumor tissues (n = 37). **D.** The overall survival analyses were plotted using Kaplan-Meier Plotter for GC patients with low or high levels of BDNF. **E.** Fluorescence in situ hybridization (FISH) staining of α-SMA and BDNF in GC tissues (200 ×). **F–H.** Immunofluorescence (IF) staining of BDNF, α-SMA, FAP, TrkB and Cytokeratin in GC tissues (200 ×). **I.** Correlation analysis of BDNF and α-SMA via TCGA data. **J.** Correlation analysis of the mRNA expression of BDNF and α-SMA in 37 pairs of GC tissues (Ruijin cohort). **K.** The mRNA expression of BNDF in CAFs, NFs, GES-1 and GC cell lines. **L-N.** Apoptosis of GC cells was detected after treatment with anlotinib (5 μM), exogenous BDNF or co-culture with CAFs transfected with BDNF/siRNA or NC/siRNA. **O-Q.** Apoptosis of GC cells was detected after treatment with anlotinib (5 μM), and/or co-culture with CAFs in the presence of IgG isotype antibody, BDNF neutralizing antibody or TrkB neutralizing antibody. Data are represented as the mean ± SD; $^{*}P < 0.05$, $^{**}P < 0.01$.

As shown in Fig. 5E–H, BDNF was mainly expressed in CAFs, while TrkB was mainly expressed in GC cells. Moreover, the expression of BDNF is significantly associated with α-SMA expression (Fig. 5I and J), and CAFs expressed higher levels of BDNF mRNA than GC cells (Fig. 5K). Thus, these findings indicate that BDNF and TrkB are coordinately overexpressed in CAFs and GC cells in human GC.

To prove that BDNF is critical to mediate CAFs-induced resistance, we further determined whether knockdown of BDNF could impair anlotinib resistance triggered by CAFs *in vitro*. As shown in Fig. 5K-M and S2A-C, the addition of exogenous BDNF or co-culture with CAFs led to resistance of anlotinib, while silencing BDNF in CAFs significantly impaired CAFs-induced resistance of anlotinib in GC cells. To further determine TrkB on GC cells as the receptor for BDNF activation of anlotinib resistance, we repeated apoptosis assays in the presence of neutralizing TrkB antibody or neutralizing BDNF antibody. As shown in Fig. 5O–Q and S2D-F, neutralization of TrkB or BDNF led to significantly decreased anlotinib resistance of GC cells induced by CAFs.

3.6. The anlotinib resistance potential of GC cells induced by CAFs-derived BDNF is mediated by the activation of Nrf2 pathway via TrkB

As anlotinib exposure induces oxidative stress and Nrf2 is a central protein in the regulation of the cellular antioxidant response, we explored whether Nrf2 pathway is involved in the regulation of anlotinib-induced oxidative stress and apoptosis by BDNF/TrkB signaling. Therefore, we determined the activation of Nrf2 in GC cells by CAFs-derived BDNF. As shown in Fig. 6A–C, exogenous BDNF or co-culture with CAFs significantly promoted the nuclear translocation of Nrf2 in GC cells. Moreover, CAFs-induced nuclear translocation of Nrf2 in GC cells could be inhibited by neutralization of TrkB or BDNF. To explore how BDNF promote Nrf2 activation, we firstly detected the mRNA level of Nrf2 after BDNF treatment. As shown in Fig. 6D–F, BDNF had no significantly effect on Nrf2 mRNA expression in anlotinib-treated GC cells, indicating that BDNF-induced activation of Nrf2 may through post-translational modifications. Keap1 is the main negative regulator of Nrf2 and Keap1-Nrf2 system plays a central role in the regulation of the levels of antioxidants, so the interaction between Nrf2 and Keap1 was examined to explore the mechanisms of BDNF in the regulation of Nrf2 pathway. Interestingly, BDNF treatment decreased Keap1-Nrf2 interaction (Fig. 6G and Fig. S3A), which caused Nrf2 activated. HO-1 is an anti-oxidant enzyme and Nrf2 is one of the key transcription factors to regulate HO-1. We found that BDNF treatment also increase the expression of HO-1 (Fig. S3B). Furthermore, exogenous BDNF or co-culture with CAFs significantly reduced anlotinib-induced ROS production, which could be significantly reversed by ML385 (a Nrf2 inhibitor) (Fig. 6H–J). In addition, exogenous BDNF or CAFs-induced resistance of anlotinib also could be inhibited by ML385 (Fig. S3C and Fig. 6K-M). Taken together, these data indicate that BDNF/TrkB signaling protects GC cells from anlotinib-induced ROS through activation of Nrf2.

3.7. GC cell-derived lactate promotes BDNF expression in CAFs via activation of NF-κB

To unravel the regulatory mechanisms of BDNF overexpression in GC, we examined the cross-talk between GC cells and CAFs. Lactate is largely produced within the tumor microenvironment (TME) by cells exploiting aerobic glycolysis (Warburg metabolism) [23]. Drug-resistant cells often exhibit high levels of Warburg metabolism, resulting in elevated production and secretion of lactate [24–26]. Lactate is an important regulator to activate CAFs [16]. Therefore, we examined whether lactate induces BDNF overexpression in CAFs. As shown in Fig. 7A and B, lactate and GC cells significantly increased the expression of BDNF in CAFs detected by qRT-PCR and ELISA. However, GC cells-induced BDNF increase was reversed by pretreatment of LDHA inhibitor (GSK 2837808A) in GC cells. It was previously reported that lactate stimulates the NF-κB pathway by triggering IκBα degradation [16,27], we next explored if lactate-induced BDNF overexpression in CAFs was mediated by this transcription factor. We found that exogenous lactate or co-culture with GC cells could significantly promote the nuclear translocation of p65 in CAFs (Fig. 7C), which indicated the activation of NF-κB pathway. Moreover, the nuclear translocation of p65 in CAFs induced by GC cells was significantly reversed by LDHA inhibitor. Above results were further confirmed by IF (Fig. S4 and 7D). Meanwhile, western blot analysis showed a decrease of IκBα, as well as

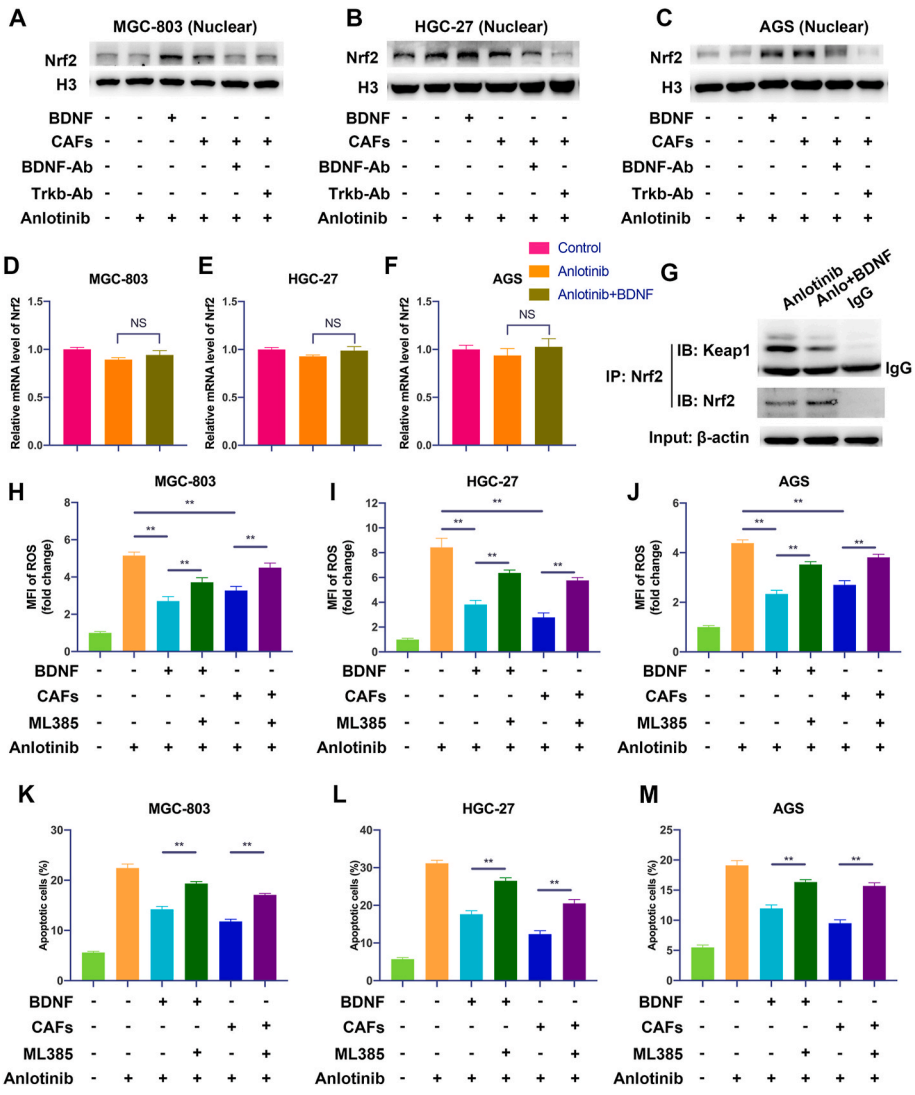

Fig. 6. The anlotinib resistance potential of GC cells induced by CAFs-derived BDNF is mediated by the activation of Nrf2 pathway via TrkB. A-C. The expression of nuclear Nrf2 in GC cells cultured in indicated conditions was analyzed by Western Blot. **D-F.** The mRNA level of Nrf2 was detected by qRT-PCR in GC cells after anlotinib or anlotinib plus BDNF treatment. **G.** Immunoprecipitation assay was performed to detect the binding between Nrf2 and Keap1 in MGC-803 cells treated with anlotinib alone or combination of anlotinib and BDNF. **H-J.** After treatment with anlotinib (5 μM), exogenous BDNF or co-culture with CAFs in the presence or absence with ML385 (a Nrf2 inhibitor), the endogenous ROS in GC cells was detected by flow cytometry. **K-M.** Apoptosis of GC cells was detected after treated with anlotinib (5 μM), exogenous BDNF or co-cultured with CAFs in the presence or absence with ML385. The data are presented as the mean ± SD from three independent experiments (*$p < 0.05$; **$p < 0.01$).

an increase of NF-κB levels in CAFs (Fig. 7E). We then used NF-κB specific inhibitor IKK-16 to interrupt NF-κB pathway, and the results revealed that CAFs treatment with IKK-16 significantly reduced lactate-induced BDNF upregulation in CAFs (Fig. 7F). These results show that NF-κB is required for BDNF overexpression induced by lactate in CAFs.

To further elucidate the mechanisms that NF-κB promotes the expression of BDNF in CAFs, we performed Chip-PCR and constructed firefly luciferase reporter-gene plasmids expressing full length or truncated BDNF promoter. As shown in Fig. 7G, NF-κB could bind BDNF promoter. Moreover, the relative luciferase activity was higher in 293T/p65 cells co-transfected with BDNF promoter (−1000~+249bp, −232~+249bp and −1000~-199bp) than that in control cells (vector) (Fig. 7H). Taken together, these results prove that GC cell-derived lactate promotes BDNF expression in CAFs via activation of NF-κB.

3.8. Inhibition of BDNF/TrkB pathway attenuates CAFs-induced protection from anlotinib of GC cells in human patient-derived organoid model

In general, patient-derived organoids (PDOs) are 3D cultures composed of multiple organ-specific cell types that can recapitulate the architecture and gene expression profiles as well as some key features and functions of their corresponding organs. Multiple studies have now identified that PDOs are robust tools to mimic the drug responsiveness in gastrointestinal cancers [28–30]. In order to further confirm above protection role of CAFs in human GC, we established PDO from GC tumor tissue. Through transwell co-culture system (PDO + CAFs) (Fig. 8A), we detected cell viability and apoptosis to verify whether blocking BDNF/TrkB reversed CAFs-induced protection of GC cells from anlotinib. As shown in Fig. 8B and 8C and S5, anlotinib efficiently inhibited PDO viability and induced apoptosis, while these anti-growth effects were abrogated in the presence of CAFs. However, adding the BDNF neutralizing antibody or TrkB neutralizing antibody into the co-culture system overcame CAFs-induced protection from anlotinib in PDOs, thus proving that therapeutic intervention of BDNF/TrkB signaling between CAFs and tumor cells would provide an opportunity to overcome the acquired resistance to anlotinib in human GC.

4. Discussion

Targeted therapy is one of the major modalities of medical treatment for advanced GC, however, acquired resistance often limits the efficacy of targeted therapies for GC patients. Anlotinib is a new oral multi-targeted TKI and has shown promising antitumor effects on various cancers. Although clinical trials of anlotinib in treating GC are in progress, its clinical efficacy on GC and the regulation of GC cell response to anlotinib is remain poorly understood. The mechanisms of

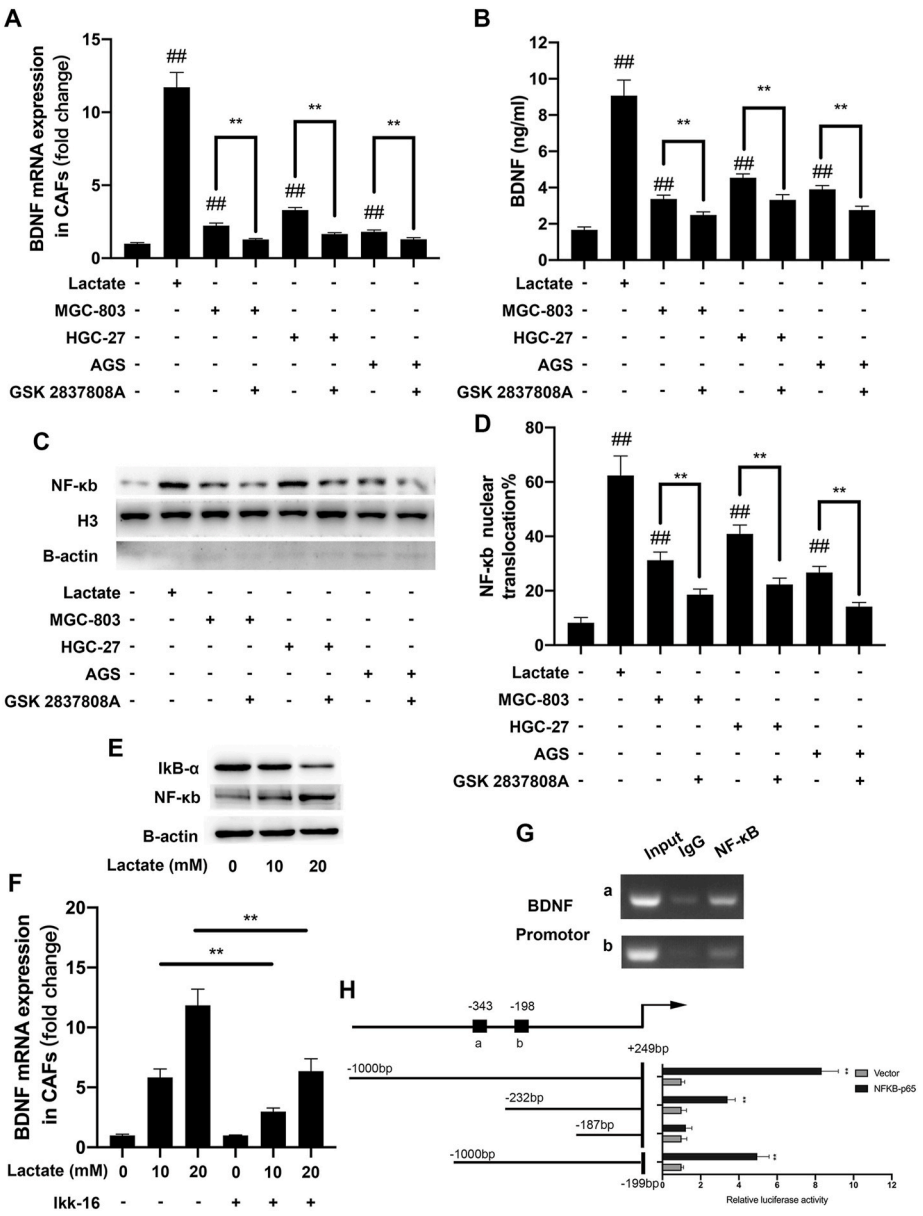

Fig. 7. GC cell-derived lactate promotes the expression of BDNF in CAFs via activation of NF-κB . A. BDNF mRNA expression in CAFs was assessed by qRT-PCR after culture in the indicated conditions. **B.** BDNF protein expression in the supernatants of CAFs was assessed by ELISA after culture in the indicated conditions. **C.** The expression of nuclear NF-κB in CAFs was detected by Western Blot in the indicated conditions. **D.** The nuclear translocation of p65 in CAFs was detected by IF. **E.** The expression of NF-κB and IkB-α in CAFs treated with indicatd concentreation of lactate were detected by Western Blot. **F.** BDNF mRNA expression in CAFs was assessed by qRT-PCR after culture in the indicated conditions. **G.** DNA fragments pulled down with NF-κB antibody in CAFs were amplified by PCR. **H.** Dual luciferase reporters containing four different truncations of the BDNF promoter region were co-transfected with NF-κB-expressing plasmid. The data are presented as the mean ± SD from three independent experiments (*$p < 0.05$; **$p < 0.01$).

acquired resistance involves both the genetic alteration of cancer cells and the interaction with their TME. CAFs, the major stromal cells in tumor microenvironment, play a key role in drug resistance via an intricate interplay of tumor microenvironment components. In this study, we demonstrated that anlotinib inhibits GC cell growth through ROS, and CAFs protect GC cells from anlotinib-induced apoptosis and induce resistance to anlotinib. Gastric CAFs express high level of BDNF, and GC cells express TrkB, which suggests that BDNF/TrkB axis may act as an important mediator of tumor-stromal cell interactions and contribute to anlotinib resistance in GC.

Anlotinib, as an anti-angiogenic drug selectively targeted to VEGFR2, has been shown broad antitumor effects through its anti-angiogenic ability. However, several studies have shown that anlotinib directly inhibits tumor cells rather than angiogenesis [4,31,32]. We here found that anlotinib directly inhibits GC cells proliferation by inducing cell apoptosis and G2/M phase arrest. Excessive levels of ROS cause cytotoxicity via regulation of DNA damage, autophagy, and metabolism, which are usually utilized by TKI drugs to kill tumor cells. ROS are the key functional regulator of TKI-induced apoptosis [33], and many TKIs are able to induce relevant mitochondrial dysfunction by uncoupling components of electron transport chain and promoting ROS generation [34]. Recent researches have shown that Dasatinib could inhibit Complex IV and Complex V, and Sorafenib could inhibit I, II + III, IV and V [35]. Gefitinib could inhibit Complex IV through induction of COX6A1 degradation, ultimately resulting in aberrant apoptosis [36]. We here demonstrated that anlotinib induced mitochondrial dysfunction related to the impairment of Complexes IV and V in the electronic respiratory chain and mitochondrial membrane depolarization. Moreover, ROS are the key mediator of anlotinib-induced apoptosis in GC cells, as abolishment of ROS by using ROS scavenger NAC significantly impaired the anti-tumor effects of anlotinib, which indicates that ROS is a mechanism utilized by anlotinib to directly induce apoptosis in GC cells.

Intrinsic or acquired resistance is a complicated and multifactorial event and remains a major challenge for the overall survival of patients with advanced GC undergoing drug therapy. A variety of factors have been demonstrated to be involved in resistance, including drug absorption, transport and efflux, the dysregulation of cell survival and death signaling pathways, cancer stemness, and TME. However, in general, our knowledge of non-cell-autonomous mechanisms of resistance is largely incomplete. Here we report for the first time that

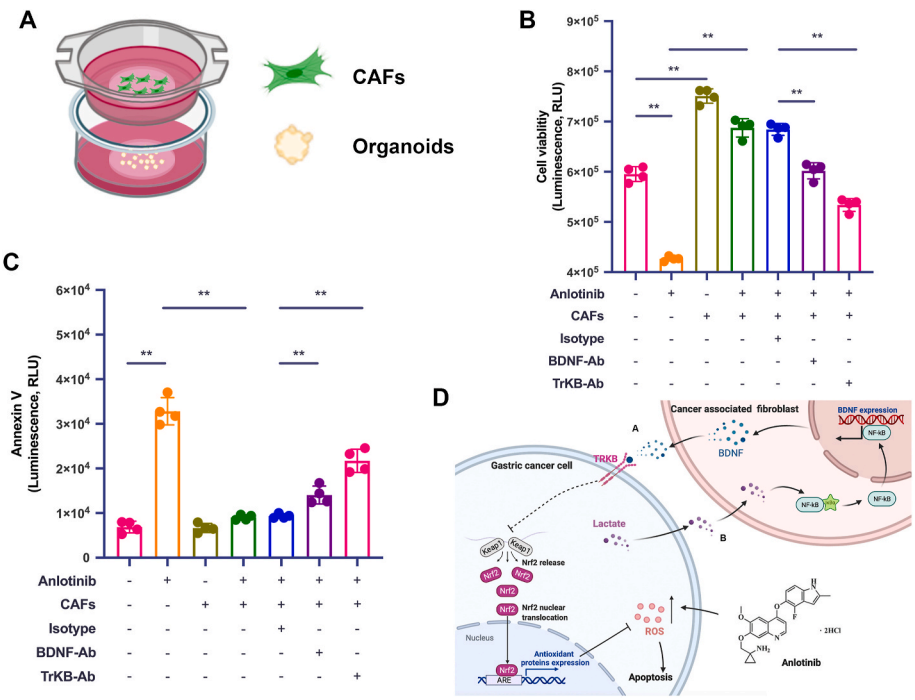

Fig. 8. Blocking BDNF/TrkB pathway inhibits CAFs-induced protection of GC cells from anlotinib in human PDO model. A. Schematic illustration of the co-culture platform. **B.** Viability assay of PDO after indicated treatments for 72 h, detected by CellTiter-Glo 3D Cell Viability Assay. **C.** Apoptosis assay of PDO after indicated treatments for 72 h, monitored by RT-Glo Annexin V. **D.** Model for the epithelial-stromal interactions in the tumor microenvironment that induces anlotinib resistance in human GC. **a.** BDNF released from CAFs reduces anlotinib-induced ROS and apoptosis of GC cells via the TrkB/Keap1-Nrf2 pathway, resulting in GC cells resistance to anlotinib. **b.** GC cell-derived lactate upregulates BDNF expression in CAFs via the NF-κB pathway. The data are presented as the mean ± SD from three independent experiments (*$p < 0.05$; **$p < 0.01$).

increased BDNF derived from CAFs reduce GC cells response to anlotinib. CAFs are the predominant cell type in tumor stroma, and contribute to tumorigenesis and progression by secreting growth factors, remolding ECM, and inducing immune evasion. We previously identified several key factors in mediating CAFs' tumor-promoting properties in GC, including IL-33, IL-6, HGF and Lumican [17–19,37]. Although BDNF has already been described in GC [22], little information is known about the role of stromal BDNF in drug resistance of GC. BDNF/TrkB signaling have been reported to be involved in apoptosis resistance or chemo-resistance in neuroblastoma, B-cell chronic lymphocytic leukemia, oesophageal cancer, head and neck squamous cell carcinoma [38–41]. In the present study, we analyzed the association of BDNF or TrkB expression with 5-fluorouracil (5-FU) response in GC, and found that BDNF or TrkB overexpression predicts lower response of 5-FU for GC patients (Fig. S6). Moreover, CAFs-derived BDNF evokes anlotinib resistance of GC cells via activation of TrkB *in vitro* and *in vivo*, and blocking BDNF/TrkB pathway is efficient to overcome CAFs-induced anlotinib resistance. To better evaluate the clinical application of these observations, treated PDO with anlotinib in the presence of CAFs, and we also found that CAFs induce anlotinib resistance, which could be attenuated by blocking BDNF/TrkB pathway. Therefore, CAFs-rich gastric cancer may be insensitive to anlotinib, and anlotinib combined with BDNF or TrkB inhibitor may be a promising strategy to treat CAFs-rich gastric cancer.

We further found that CAFs-induced anlotinib resistance are mediated by the activation of Nrf2 pathway via BDNF/TrkB signal. Nrf2 is an endogenous antioxidant that can reduce ROS to avoid excessive ROS-induced cell damage by activating downstream effectors. Previous studies have shown that trastuzumab in combination with Nrf2 inhibitor exerts synergistic antitumor activity in gastric cancer [42,43]. Compared with expression in normal samples, GC tumors have higher Nrf2 expression of transcripts, and Nrf2 expression is inversely proportional to survival in GC (Fig. S7A and S7B). Yang, etc. [31] and Sun, etc. [44] have reported that downregulating Nrf2 enhances pro-apoptotic effect of anlotinib in pancreatic cancer and non-small-cell lung cancer. Consistent with the previous studies, we also demonstrated that inhibition of Nrf2 sensitize GC cells to anlotinib treatment, which suggested combination of Nrf2 inhibition and anlotinib would provide a new and effective strategy for the treatment of GC.

Since Nrf2 activation by CAFs is observed in the anlotinib-treated GC cells and resists the anti-tumor effects of anlotinib, we therefore explored how CAFs-derived BDNF activated Nrf2. It is well known that Keap1 can bind to Nrf2 in the cytoplasm, and then inhibits the nuclear translocation of Nrf2 and promotes the ubiquitination degradation of Nrf2, thereby resisting the activation of the Nrf2 signaling pathway [45]. Indeed, BDNF treatment decreased Keap1-Nrf2 interaction and promoted the nuclear translocation of Nrf2 in anlotinib-treated GC cells (Fig. 6G). Besides, p62 interacts with the Nrf2-binding site of Keap1 and competitively inhibits the Keap1-Nrf2 interaction, which activates Nrf2 in an alternative way. Therefore, increased expression of p62 also could activate Nrf2, so we further detected the influence of BDNF in the expression for p62 and autophagy. Although anlotinib treatment decreased the expression of p62 and induced autophagy, which is consistent with other studies [32,44], BDNF treatment did not affect anlotinib-induced autophagy (Fig. S7C-F). In addition, posttranslational modification of Keap1 and Nrf2 is one of the important way to regulate the affinity between Keap1 and Nrf2 [46,47]. The Cys273 and Cys288 are key sites of Keap1 for its negative regulation of NRF2, and modification of Cys273 and Cys288 affects the interaction between Keap1 and Nrf2 [48]. The Cys151 of Keap1 also plays a key role of regulation of Nrf2 [49]. Phosphorylation of Keap1 at Ser599 and Ser602 promotes the interaction between Keap1 and Nrf2 to increase the degradation of Nrf2 [50]. Moreover, phosphorylation of Nrf2 at Ser40 also affects the interaction between Nrf2 and Keap1 [51]. Further exploration of the posttranslational modification of Keap1 and Nrf2 would better understand the mechanism how anlotinib and BDNF regulate the affinity between Keap1 and Nrf2.

Cancer cells are characterized by elevated aerobic glycolysis and increased lactate release [52]. Abundant evidences have proven that lactate regulates anti-tumor drugs response in several tumors [53–55]. Lactate is also an important mediator to rewrite TME. Increased lactate is able to activate CAFs to secrete cytokine overcoming the inhibitory effect of TKIs [16]. In the present study, we identified a critical role of GC cell-derived lactate in promoting BDNF expression of CAFs via NF-κB pathway. Targeting tumor lactate metabolism was sufficient to overcome resistance, thus demonstrating the causative role of the

lactate/BDNF axis. These data open new possible applications for targeting glycolysis in preventing/overcoming resistance onset.

Based on this study, we characterized an intricate network of the cross-talk between GC cells and CAFs that induces anlotinib resistance (Fig. 8D). We have shown that BDNF released by CAFs protects GC cells from anlotinib via TrkB, which is dependent on the activation of Nrf2 pathway. Conversely, lactate released by GC cells promotes BDNF expression in CAFs via NF-κB pathway. In conclusion, the cross-talk between tumor cells and stromal cells mediated by lactate/BDNF/TrkB signaling plays a key role in the acquired resistance to anlotinib in GC. Therefore, therapeutic intervention by targeting this forward feedback loop would provide an alternative strategy to sensitize GC cells to anlotinib treatment and achieve long-term efficacy in human GC.

Declaration of competing interest

The authors declare no potential conflicts of interest.

Acknowledgments

This work was supported by the National Natural Science Foundation of China (No. 81871902 and No. 82072616), Shanghai Municipal Education Commission-Gaofeng Clinical Medicine Grant Support (No. 20152505), China Scholarship Council (201906230139), and Shanghai Sailing Program (No. 21YF1427600).

Appendix A. Supplementary data

Supplementary data to this article can be found online at https://doi.org/10.1016/j.redox.2021.102076.

References

[1] H. Sung, et al., Global cancer statistics 2020: GLOBOCAN estimates of incidence and mortality worldwide for 36 cancers in 185 countries, Ca - Cancer J. Clin. 71 (3) (2021) 209–249.
[2] C. Xie, et al., Preclinical characterization of anlotinib, a highly potent and selective vascular endothelial growth factor receptor-2 inhibitor, Canc. Sci. 109 (4) (2018) 1207–1219.
[3] Y.Y. Syed, Anlotinib: first global approval, Drugs 78 (10) (2018) 1057–1062.
[4] G. Wang, et al., Anlotinib, a novel small molecular tyrosine kinase inhibitor, suppresses growth and metastasis via dual blockade of VEGFR2 and MET in osteosarcoma, Int. J. Canc. 145 (4) (2019) 979–993.
[5] X.Z. Chen, Anlotinib for refractory advanced non-small cell lung cancer in China, JAMA Oncol 5 (1) (2019) 116–117.
[6] M. Zhou, et al., China National Medical Products Administration approval summary: anlotinib for the treatment of advanced non-small cell lung cancer after two lines of chemotherapy, Canc. Commun. 39 (1) (2019) 36.
[7] F. Song, et al., Anlotinib suppresses tumor progression via blocking the VEGFR2/PI3K/AKT cascade in intrahepatic cholangiocarcinoma, Cell Death Dis. 11 (7) (2020) 573.
[8] L. Tang, et al., Anlotinib inhibits synovial sarcoma by targeting GINS1: a novel downstream target oncogene in progression of synovial sarcoma, Clin. Transl. Oncol. 21 (12) (2019) 1624–1633.
[9] C. He, T. Wu, Y. Hao, Anlotinib induces hepatocellular carcinoma apoptosis and inhibits proliferation via Erk and Akt pathway, Biochem. Biophys. Res. Commun. 503 (4) (2018) 3093–3099.
[10] Y. Chi, et al., Safety and efficacy of anlotinib, a multikinase angiogenesis inhibitor, in patients with refractory metastatic soft-tissue sarcoma, Clin. Canc. Res. 24 (21) (2018) 5233–5238.
[11] J. Wang, et al., Anlotinib combined with SOX regimen (S1 (tegafur, gimeracil and oteracil porassium capsules) + oxaliplatin) in treating stage IV gastric cancer: study protocol for a single-armed and single-centred clinical trial, BMJ Open 10 (6) (2020), e034685.
[12] Y. Wu, et al., Comprehensive genomic meta-analysis identifies intra-tumoural stroma as a predictor of survival in patients with gastric cancer, Gut 62 (8) (2013) 1100–1111.
[13] D. Lee, et al., Intratumor stromal proportion predicts aggressive phenotype of gastric signet ring cell carcinomas, Gastric Cancer 20 (4) (2017) 591–601.
[14] N.A. Bhowmick, E.G. Neilson, H.L. Moses, Stromal fibroblasts in cancer initiation and progression, Nature 432 (7015) (2004) 332–337.
[15] S.L. Shiao, et al., Immune microenvironments in solid tumors: new targets for therapy, Genes Dev. 25 (24) (2011) 2559–2572.
[16] M. Apicella, et al., Increased lactate secretion by cancer cells sustains non-cell-autonomous adaptive resistance to MET and EGFR targeted therapies, Cell Metabol. 28 (6) (2018) 848–865 e6.
[17] X. Wu, et al., IL-6 secreted by cancer-associated fibroblasts promotes epithelial-mesenchymal transition and metastasis of gastric cancer via JAK2/STAT3 signaling pathway, Oncotarget 8 (13) (2017) 20741–20750.
[18] X. Wu, et al., Hepatocyte growth factor activates tumor stromal fibroblasts to promote tumorigenesis in gastric cancer, Canc. Lett. 335 (1) (2013) 128–135.
[19] Q. Zhou, et al., The reciprocal interaction between tumor cells and activated fibroblasts mediated by TNF-alpha/IL-33/ST2L signaling promotes gastric cancer metastasis, Oncogene 39 (7) (2020) 1414–1428.
[20] Z. Jin, et al., FGFR3 big up tri, open7-9 promotes tumor progression via the phosphorylation and destabilization of ten-eleven translocation-2 in human hepatocellular carcinoma, Cell Death Dis. 11 (10) (2020) 903.
[21] T. Pan, et al., Cathepsin L promotes angiogenesis by regulating the CDP/Cux/VEGF-D pathway in human gastric cancer, Gastric Cancer 23 (6) (2020) 974–987.
[22] Y. Okugawa, et al., Brain-derived neurotrophic factor/tropomyosin-related kinase B pathway in gastric cancer, Br. J. Canc. 108 (1) (2013) 121–130.
[23] L. Ippolito, et al., Lactate: a metabolic driver in the tumour landscape, Trends Biochem. Sci. 44 (2) (2019) 153–166.
[24] M. Bacci, et al., miR-155 drives metabolic reprogramming of ER+ breast cancer cells following long-term estrogen deprivation and predicts clinical response to aromatase inhibitors, Canc. Res. 76 (6) (2016) 1615–1626.
[25] I.L. Lai, et al., Targeting the Warburg effect with a novel glucose transporter inhibitor to overcome gemcitabine resistance in pancreatic cancer cells, Carcinogenesis 35 (10) (2014) 2203–2213.
[26] M. Zhou, et al., Warburg effect in chemosensitivity: targeting lactate dehydrogenase-A re-sensitizes taxol-resistant cancer cells to taxol, Mol. Canc. 9 (2010) 33.
[27] F. Vegran, et al., Lactate influx through the endothelial cell monocarboxylate transporter MCT1 supports an NF-kappaB/IL-8 pathway that drives tumor angiogenesis, Canc. Res. 71 (7) (2011) 2550–2560.
[28] P. Roy, et al., Organoids as preclinical models to improve intraperitoneal chemotherapy effectiveness for colorectal cancer patients with peritoneal metastases: preclinical models to improve HIPEC, Int. J. Pharm. 531 (1) (2017) 143–152.
[29] M. Crespo, et al., Colonic organoids derived from human induced pluripotent stem cells for modeling colorectal cancer and drug testing, Nat. Med. 23 (7) (2017) 878–884.
[30] H.H.N. Yan, et al., A comprehensive human gastric cancer organoid biobank captures tumor subtype heterogeneity and enables therapeutic screening, Cell Stem Cell 23 (6) (2018) 882–897 e11.
[31] L. Yang, et al., Reactive oxygen species mediate anlotinib-induced apoptosis via activation of endoplasmic reticulum stress in pancreatic cancer, Cell Death Dis. 11 (9) (2020) 766.
[32] L. Liang, et al., Autophagy inhibition potentiates the anti-angiogenic property of multikinase inhibitor anlotinib through JAK2/STAT3/VEGFA signaling in non-small cell lung cancer cells, J. Exp. Clin. Canc. Res. 38 (1) (2019) 71.
[33] M.E. Grabowska, et al., Computational model of cardiomyocyte apoptosis identifies mechanisms of tyrosine kinase inhibitor-induced cardiotoxicity, J. Mol. Cell. Cardiol. 155 (2021) 66–77.
[34] M.A. Rodriguez-Hernandez, et al., Integrated molecular signaling involving mitochondrial dysfunction and alteration of cell metabolism induced by tyrosine kinase inhibitors in cancer, Redox Biol 36 (2020) 101510.
[35] Y. Will, et al., Effect of the multitargeted tyrosine kinase inhibitors imatinib, dasatinib, sunitinib, and sorafenib on mitochondrial function in isolated rat heart mitochondria and H9c2 cells, Toxicol. Sci. 106 (1) (2008) 153–161.
[36] P. Luo, et al., PLK1 (polo like kinase 1)-dependent autophagy facilitates gefitinib-induced hepatotoxicity by degrading COX6A1 (cytochrome c oxidase subunit 6A1), Autophagy (2020) 1–17.
[37] X. Wang, et al., Cancer-associated fibroblast-derived Lumican promotes gastric cancer progression via the integrin beta1-FAK signaling pathway, Int. J. Canc. 141 (5) (2017) 998–1010.
[38] K. Tanaka, et al., Neurotrophic receptor, tropomyosin-related kinase B, as a chemoresistant marker in oesophageal cancer, Clin. Oncol. 21 (4) (2009) 362–363.
[39] J. Lee, T. Jiffar, M.E. Kupferman, A novel role for BDNF-TrkB in the regulation of chemotherapy resistance in head and neck squamous cell carcinoma, PLoS One 7 (1) (2012), e30246.
[40] A. Abbaci, et al., Neurotensin receptor type 2 protects B-cell chronic lymphocytic leukemia cells from apoptosis, Oncogene 37 (6) (2018) 756–767.
[41] Z. Li, F. Tan, C.J. Thiele, Inactivation of glycogen synthase kinase-3beta contributes to brain-derived neutrophic factor/TrkB-induced resistance to chemotherapy in neuroblastoma cells, Mol. Canc. Therapeut. 6 (12 Pt 1) (2007) 3113–3121.
[42] V. Gambardella, et al., NRF2 through RPS6 activation is related to anti-HER2 drug resistance in HER2-amplified gastric cancer, Clin. Canc. Res. 25 (5) (2019) 1639–1649.
[43] Y. Yang, et al., Nrf2 inhibitor, brusatol in combination with trastuzumab exerts synergistic antitumor activity in HER2-positive cancers by inhibiting Nrf2/HO-1 and HER2-AKT/ERK1/2 pathways, Oxid Med Cell Longev 2020 (2020) 9867595.
[44] X. Sun, et al., Transcriptome profiling analysis reveals that ATP6V0E2 is involved in the lysosomal activation by anlotinib, Cell Death Dis. 11 (8) (2020) 702.
[45] M. Yamamoto, T.W. Kensler, H. Motohashi, The KEAP1-NRF2 system: a thiol-based sensor-effector apparatus for maintaining redox homeostasis, Physiol. Rev. 98 (3) (2018) 1169–1203.
[46] Y. Huang, et al., The complexity of the Nrf2 pathway: beyond the antioxidant response, J. Nutr. Biochem. 26 (12) (2015) 1401–1413.
[47] L. Baird, M. Yamamoto, The molecular mechanisms regulating the KEAP1-NRF2 pathway, Mol. Cell Biol. 40 (13) (2020).

[48] N. Wakabayashi, et al., Protection against electrophile and oxidant stress by induction of the phase 2 response: fate of cysteines of the Keap1 sensor modified by inducers, Proc. Natl. Acad. Sci. U. S. A. 101 (7) (2004) 2040–2045.
[49] A.L. Eggler, et al., Identification of the highly reactive cysteine 151 in the chemopreventive agent-sensor Keap1 protein is method-dependent, Chem. Res. Toxicol. 20 (12) (2007) 1878–1884.
[50] S.K. Niture, A. Gnatt, A.K. Jaiswal, Oncogene PKCepsilon controls INrf2-Nrf2 interaction in normal and cancer cells through phosphorylation of INrf2, J. Cell Sci. 126 (Pt 24) (2013) 5657–5669.
[51] D.A. Bloom, A.K. Jaiswal, Phosphorylation of Nrf2 at Ser40 by protein kinase C in response to antioxidants leads to the release of Nrf2 from INrf2, but is not required for Nrf2 stabilization/accumulation in the nucleus and transcriptional activation of antioxidant response element-mediated NAD(P)H:quinone oxidoreductase-1 gene expression, J. Biol. Chem. 278 (45) (2003) 44675–44682.
[52] R.A. Cairns, I.S. Harris, T.W. Mak, Regulation of cancer cell metabolism, Nat. Rev. Canc. 11 (2) (2011) 85–95.
[53] E.M.E. Barnes, et al., Lactic acidosis induces resistance to the pan-Akt inhibitor uprosertib in colon cancer cells, Br. J. Canc. 122 (9) (2020) 1298–1308.
[54] S. Park, et al., ERRalpha-regulated lactate metabolism contributes to resistance to targeted therapies in breast cancer, Cell Rep. 15 (2) (2016) 323–335.
[55] E. Allen, et al., Metabolic symbiosis enables adaptive resistance to anti-angiogenic therapy that is dependent on mTOR signaling, Cell Rep. 15 (6) (2016) 1144–1160.